REPORT DOCUMENTATION PAGE

Form Approved OMB No. 0704-0188

Public reporting burden for this collection of information is estimated to average 1 hour per response, including the time for reviewing instructions, searching existing data sources, gathering and maintaining the data needed, and completing and reviewing the collection of information. Send comments regarding this burden estimate or any other aspect of this collection of information, including suggestions for reducing the burden, to Department of Defense, Washington Headquarters Services, Directorate for Information Operations and Reports (0704-0188), 1215 Jefferson Davis Highway, Suite 1204, Arlington, VA 22202-4302. Respondents should be aware that notwithstanding any other provision of law, no person shall be subject to any penalty for failing to comply with a collection of information if it does not display a currently valid OMB control number.
PLEASE DO NOT RETURN YOUR FORM TO THE ABOVE ADDRESS.

1. REPORT DATE *(DD-MM-YYYY)*
18-08-2004

2. REPORT TYPE
Final Report

3. DATES COVERED *(From – To)*
1 October 2003 - 01-Oct-04

4. TITLE AND SUBTITLE
Numerical Modeling Of Penetration Into A Compressible Viscoplastic Media

5a. CONTRACT NUMBER
FA8655-03-M4080

5b. GRANT NUMBER

5c. PROGRAM ELEMENT NUMBER

6. AUTHOR(S)
Professor Ioan R Ionescu

5d. PROJECT NUMBER

5d. TASK NUMBER

5e. WORK UNIT NUMBER

7. PERFORMING ORGANIZATION NAME(S) AND ADDRESS(ES)
Universite de Savoie
Campus Scientifique
Le Bourget-du-Lac 73376
France

8. PERFORMING ORGANIZATION REPORT NUMBER
N/A

9. SPONSORING/MONITORING AGENCY NAME(S) AND ADDRESS(ES)
EOARD
PSC 802 BOX 14
FPO 09499-0014

10. SPONSOR/MONITOR'S ACRONYM(S)

11. SPONSOR/MONITOR'S REPORT NUMBER(S)
SPC 03-4080

12. DISTRIBUTION/AVAILABILITY STATEMENT
Approved for public release; distribution is unlimited.

13. SUPPLEMENTARY NOTES

14. ABSTRACT

This report results from a contract tasking Universite de Savoie as follows: The contractor will develop new computational techniques and use them to gain fundamental understanding of the physical phenomena associated with penetration into a semi-infinite geological target of a hard (rigid) penetrator at intermediate impact velocities (typically, below 1000 m/s). The contractor we will implement viscoplastic models accounting for the combined effects of high strain rate and high confinement on the response of geologic and cementitious materials. The focus will be on capturing increased hardening with compaction; diminished strain rate sensitivity with compaction; damage induced anisotropy; non-symmetrical strength effects in the target material and how these target properties affect the penetrator performance. Predictive capabilities for describing separation and damage ahead of the projectile will also result from this investigation.

15. SUBJECT TERMS
EOARD, Fracture mechanics, Metals & alloys, High Strain Rate , Penetrator

16. SECURITY CLASSIFICATION OF:			17. LIMITATION OF ABSTRACT	18, NUMBER OF PAGES	19a. NAME OF RESPONSIBLE PERSON
a. REPORT	b. ABSTRACT	c. THIS PAGE			KEVIN J LAROCHELLE, Maj, USAF
UNCLAS	UNCLAS	UNCLAS	UL	19	19b. TELEPHONE NUMBER *(Include area code)* +44 (0)20 7514 3154

Standard Form 298 (Rev. 8/98)
Prescribed by ANSI Std. Z39-18

Numerical modeling of penetration into compressible viscoplastic media
FINAL REPORT

EOARD: No. FA8655-03-M-4080, PI: Ioan R. Ionescu[†]

22nd July 2004

[†] Laboratoire de Mathématiques, Université de Savoie, Campus Scientifique,
73376 Le Bourget-du-Lac Cedex, France, Fax 33.4.79.75.81.42, ionescu@univ-savoie.fr

Abstract

Computational methods for simulation of the tunneling stage of penetration into semi-infinite compressible geological targets of a hard (rigid) penetrator for intermediate impact velocities (typically, below 1000 m/s) were developed. A compressible viscoplastic fluid constitutive equation that captures the combined effects of high-strain rate and high-pressure (confinement)on yielding was developed. To account for the experimentally observed characteristics of the response at high-pressures the hypothesis of a locking medium was adopted (i.e. the density cannot exceed a critical limit). To simulate steady-state penetration, a mixed finite-element and finite-volume strategy is developed. Specifically, the variational inequality for the velocity field is discretized using the finite element method and a finite volume method is adopted for the density equation. To solve the velocity problem a decomposition-coordination formulation coupled with the augmented lagrangian method is used. This approach is accurate in detecting the visco-plastic regions and permit us to handle the locking condition. The ability of the proposed model to accurately describe (i) the density changes in the target around the penetration tunnel, ii) the shape and location of rigid/plastic boundary, iii) the directional damage/fracture ahead of the penetrator. Moreover the fact that fracture occurs ahead of the penetrator and along planes which are not symmetric with respect to the penetrator centerline, can explain trajectory instabilities.

Contents

1 Introduction **2**

2 Material modeling **3**

3 Statement of the problem **5**

4 Numerical approach **7**
4.1 The velocity problem 7
4.2 The density problem 9

5 Penetration in concrete **10**
5.1 Material parameters model 10
5.2 Boundary conditions 11
5.3 Mesh adaptation 11

6 Results and discussion **13**

7 Conclusions **17**

1 Introduction

Kinetic energy penetration phenomena are of interest in a variety of applications ranging from terminal ballistics to protection of spacecraft due to meteoroid impact, containment of high mass or high velocity debris due to accidents or high rate energy release, design of hardened protective facilities, erosion and fracture of solids due to impact, *etc.* (Zukas [32]). The occurrence of multiple phenomena in the target such as localization, plasticity, anisotropic damage, fragmentation pushes the limits of existing modelling and computational capabilities for description of the target response.

Since the deformation rates are very large (of the order of $10^5 s^{-1}$), a fluid formulation in eulerian description could describe the main features of the target deformation. Because shear flow takes place only if a certain threshold is surpassed, a non-newtonian fluid model is not appropriate. Since yielding cannot be neglected, viscoplastic fluid models such as Bingham have been used [2, 9, 17, 18] in studies concerning penetration into metalic targets. It is to be noted that such models are suitable for the description of the high-strain rate behavior of metals for which yielding is insensitive to pressure and consequently are incompressible. As opposed to metals, in geological materials yielding is pressure-dependent (e.g. [27]). For these materials, compressibility is not a second order property as for non-newtonian fluids. Indeed, the geologic and cementitious materials have a compaction rate up to 30% and their mechanical properties (viscosity, yield limit, etc) depend significantly on density (4 to 400 times increase in yield limit for quasi-static and dynamic conditions, respectively). Thus, compressible viscoplastic fluid models should be considered.

Only a limited number of 2-D and 3-D calculations of penetration into cementitious or geologic materials for low to intermediate velocity impacts have been reported in the open literature. Finite-element and finite-difference models employing both Lagrangian and Eulerian formulations have been used. Each of these methods has advantages and disadvantages as a tool to model penetration. For example, with the finite-element method using Lagrangian formulation, one needs to perform a remeshing whenever the mesh becomes highly distorted as the projectile advances in the target. A finite-difference method generally utilizes an Eulerian description in which the mesh is fixed in space, and thus does not distort. The moving boundary between the penetrator and the surrounding target is not sharp, and special interface tracking methods are required (e.g. level set methods). Mesh-less methods have also been proposed for tracking moving fronts of discontinuities.

In discrete element models (DEM) the material is treated as heterogeneous at the macroscale. Specifically, the material is discretized into individual elements or blocks, which are allowed to interact as stress is applied [23]. Applications of DEM to modelling the dynamic behavior of concrete have been reported [6, 10] and a very good agreement with experiments was obtained. However, DEM is not applicable to large scale problems because the computation time required to solve even simple, routine problems can be excessive.

It is to be noted that the material models used in conjunction with the aforementioned methods exhibit limited features such as pressure-dependent yield surfaces (e.g. Schwer et al. [27]), strain-rate dependent yield surfaces (e.g. Batra [2]), pressure and strain-rate dependent yield surfaces (e.g. Adamik and Matejovic, [1]), simple equations of state for porous materials models (e.g. Tipton [31]). Most of the material models are incompressible.

A new model for describing steady-state penetration in geological or geologically derived materials is presented in this paper which is outlined as follows. To account for the combined effects of high-pressure and high strain-rate on the flow behavior, a new constitutive equation

is proposed in section 2. The focus is on capturing the increase in the yielding limit with the degree of compaction as well as the observed decrease in strain rate sensitivity. Since in the range of impact velocities of interest, the target material displays both solid-like and fluid-like behavior, the material model will be obtained by superposing a rigid-plastic solid to a compressible viscous fluid.

The problem statement of steady state penetration and its variational formulations are presented in section 3. A mixed finite-element and finite-volume strategy is developed in section 4. Specifically, the variational inequality for the velocity field is discretized using the finite element method and a finite volume method is adopted for the density equation. To solve the velocity problem a mixed formulation with the augmented lagrangian method is used. The model is further applied to axisymmetric penetration into concrete in section 5. The material parameters are found following the recent experimental data obtained by Schmidt [29]. In order to capture sharply the shape of the visco-plastic zone, we have used an anisotropic mesh generator. The model predicts that around the penetrator, a fully compacted state is achieved, the maximum compaction being in the nose zone. Fracture occurs ahead of the penetrator and along planes which can be not symmetric with respect to the penetrator centerline. This induced anisotropy can explain trajectory deviations

2 Material modeling

In the hypervelocity impact range, the flow behavior of the target could be described accurately by classic fluid type constitutive equations. At low-to-intermediate impact velocity (below 1000 m/s), the impacted medium may display both solid and fluid-like properties. Thus, model for fluids with yield limit are generally used. Since yielding of metals is insensitive to pressure, these models are incompressible (e.g. Bingham type constitutive equation) [2, 9, 17, 18]). In contrast, for geological materials yielding is pressure-dependent (e.g. [27]). The effect of the density on flow cannot be neglected, since compressibility is not a second- order property as for non-newtonian fluids. Thus, a compressible Bingham type model with yielding dependent on the actual density (or compaction level) needs to be considered.

Let denote by $\boldsymbol{u}$ the material velocity, by D the rate of deformation tensor and by $D' = D - \frac{1}{3}(\operatorname{tr} D)I_3$ its deviator

$$D = D(\boldsymbol{u}) = \frac{1}{2}(\nabla \boldsymbol{u} + \nabla^T \boldsymbol{u}), \quad D' = D'(\boldsymbol{u}) = D(\boldsymbol{u}) - \frac{1}{3}\operatorname{div} \boldsymbol{u} I_3. \tag{1}$$

Also, the Cauchy stress tensor is denoted by $\boldsymbol{\sigma}$ and its deviator by $\boldsymbol{\sigma}' = \boldsymbol{\sigma} - \operatorname{tr} \boldsymbol{\sigma} I_3$. In contrast to a Navier-Stokes fluid, a classic Bingham fluid (see [3, 22, 8]), can sustain a shear stress even at rest and it starts to flow only if the applied forces exceed an *yield limit* κ. To account for the effect of compaction on the deviatoric response of cementitious or geologic materials, in [4] the yield limit κ was considered to be a function of the current density. In this paper, we consider an extension (see [11]) of the Bingham model which is obtained by superposing a rigid-plastic solid to a compressible viscous fluid, i.e.

$$\boldsymbol{\sigma} = S + [-p(\rho) + \lambda(\rho)(\operatorname{tr} D)]I_3 + 2\eta(\rho)D \tag{2}$$

$$\mathcal{F}(S, \rho) \leq 0 \tag{3}$$

$$D' = \mu \partial_S \mathcal{F} \tag{4}$$

where the tensor S is the part of the stress which describes the plastic properties of the material, ρ is the density while $\eta, \lambda > 0$, are *viscosity coefficients*, $\mathcal{F}$ is the *yield function* and μ is a scalar function such that

$$\begin{array}{ll} \mu(t) = 0 & \text{if } \mathcal{F}(S,\rho) < 0 \text{ or } \mathcal{F}(S,\rho) = 0 \text{ and } \partial_S \mathcal{F}(S,\rho) : \dot{S} < 0 \\ \mu(t) > 0 & \text{if } \mathcal{F}(S,\rho) = 0 \text{ and } \partial_S \mathcal{F}(S,\rho) : \dot{S} = 0 \end{array} \tag{5}$$

Note that the viscosity coefficients η, λ as well as the yield function $\mathcal{F}$ are considered to be functions of the current density ρ or alternatively on the compaction factor $c = \rho/\rho_0 - 1$.

Further, it will be assumed that the *Mises condition* is satisfied, i.e.

$$\mathcal{F}(S) = |S'|^2 - \kappa^2(\rho), \tag{6}$$

where $\kappa^2(\rho)$ is the yield limit in shear which is considered to be a function of the current density. Experimental studies of the dynamic behavior of cementitious materials have indicated a strong dependence of yielding and subsequent flow on density (see for instance experimental data on cementitious materials reported in [21, 26, 28]).

The material function $p(\rho)$, describes the volumetric response of the material. Under hydrostatic conditions, most cementitious materials show a highly non-linear pressure-volumetric strain response, the reversible decrease in volume being very small. The experimental observations also suggest that in the high-pressure regime, a very large increase in pressure is necessary in order to produce even a very small change in density. Thus, the hypothesis of a "locking medium" can be made, i.e. the density cannot exceed a critical value. This critical density ρ^*, called locking density, corresponds to a state in the material when all the pores and cracks are closed. The pressure level at which this density is first reached, called locking pressure, is denoted by $p^* = p(\rho^*)$. Hence,

$$\begin{cases} p &= p(\rho), \qquad \text{if } \rho < \rho* \\ p &\geq p^*, \qquad \text{if } \rho = \rho^* \end{cases} \tag{7}$$

Since during unloading the reversible decrease of volume is very small, it can be neglected and therefore the unloading process is rigid. Hence,

$$\operatorname{tr} D \leq 0, \qquad \begin{cases} \operatorname{tr} S = 0, & \text{if } \operatorname{tr} D < 0 \\ \operatorname{tr} S \geq 0, & \text{if } \operatorname{tr} D = 0. \end{cases} \tag{8}$$

Following the procedure used to construct the classical Bingham fluid (see [8]), from equations (2) to (5) we deduce the relationship between the deviatoric part of the rate of deformation and the stress deviator:

$$D' = \begin{cases} \dfrac{1}{2\eta(\rho) + a}\left(1 - \dfrac{\kappa(\rho)}{|\boldsymbol{\sigma}'|}\right)\boldsymbol{\sigma}' & \text{if } |\boldsymbol{\sigma}'| > \kappa(\rho) \\ 0 & \text{if } |\boldsymbol{\sigma}'| \leq \kappa(\rho). \end{cases} \tag{9}$$

Next, by inverting the constitutive equation (9) we obtain that the shear response is governed by

$$\begin{cases} \boldsymbol{\sigma}' = 2\eta(\rho)D' + \kappa(\rho)\dfrac{D'}{|D'|} & \text{if } |D'| \neq 0 \\ |\boldsymbol{\sigma}'| \leq \kappa(\rho) & \text{if } |D'| = 0. \end{cases} \tag{10}$$

The formulation of the model is completed by providing the equations governing the response under hydrostatic conditions. From (2) and (8)

$$\begin{cases} \operatorname{tr}\boldsymbol{\sigma} = -3p(\rho) + \big(3\lambda(\rho) + 2\eta(\rho)\big)\operatorname{tr} D & \text{if } \operatorname{tr} D < 0 \\ \operatorname{tr}\boldsymbol{\sigma} \geq -3p(\rho) & \text{if } \operatorname{tr} D = 0. \end{cases} \tag{11}$$

Subsequently we will refer to (10)-(11) as the constitutive equations of the compressible Bingham-type material. Note that the classical Bingham fluid (1) is recovered if in (10) the incompressibility condition (i.e. $\operatorname{div}\boldsymbol{u} = 0$) is imposed.

3 Statement of the problem

In this section we present the equations governing the steady-state motion of concrete, described by the constitutive equation (10)-(11), over a rigid penetrator fully embedded in the target, represented by a domain $\mathcal{D} \subset \mathbb{R}^3$ with a smooth boundary $\partial\mathcal{D}$.

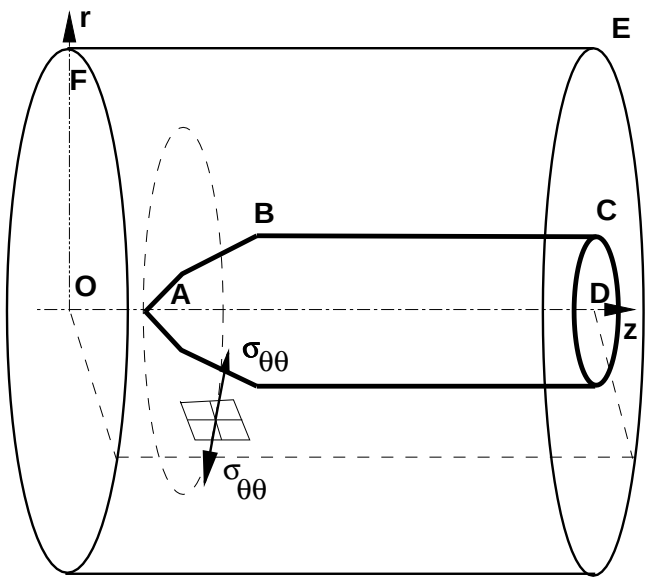

Figure 1: A schematic representation of the domain $\mathcal{D}$.

The domain $\mathcal{D}$ is assumed to be the whole space $\mathbb{R}^3$ without the penetrator $\mathcal{P}$ and the infinite tunnel $\mathcal{T}$ behind it. $\partial_0\mathcal{D}$ where the velocities $\mathbf{V}$ are prescribed will be the infinity of the domain $\mathcal{D}$; $\partial_1\mathcal{D}$ is the boundary of the tunnel while $\partial_2\mathcal{D}$, is the part of the boundary where there is frictional contact with the projectile. However, post-test observations indicate that the tunnel is of the order of the projectile diameter. For both grout and concrete targets a change in density in the region around the penetration tunnel radially outward from the edge of the tunnel to a distance of $1 - 1.5$ projectile diameters was reported (see Jones et al [19]). Hence, the domain affected by the impact event is bounded and thus $\mathcal{D}$ will be restricted to the domain shown Figure 1. To enable reasonable computational effort and still ensure that the boundary conditions at infinity are accurately described, we limit the extent of this

domain to 5 projectile radii. The projectile is considered to be rigid and axisymmetric. Since, at striking velocities up to 1200 m/s, penetration paths are relatively straight and stable with regard to the original shotline, the problem could be considered axisymmetric with respect to the projectile centerline $0z$.

The momentum balance law in the Eulerian coordinates reads

$$\rho(\boldsymbol{u}\cdot\nabla)\boldsymbol{u} - \mathbf{div}\,\boldsymbol{\sigma} = \rho\boldsymbol{f} \quad \text{in } \mathcal{D}, \tag{12}$$

where $\rho = \rho(x) \geq \rho_0 > 0$ is the mass density distribution and $\boldsymbol{f}$ denotes the body forces. The continuity equation is

$$\operatorname{div}(\rho\boldsymbol{u}) = 0 \quad \text{in } \mathcal{D}. \tag{13}$$

To the system of equations (10)-(11)and (12)we associate the following boundary conditions:

$$\boldsymbol{u} = \mathbf{V} \quad \text{on} \quad \partial_0\mathcal{D}, \quad \boldsymbol{\sigma n} = 0 \quad \text{on} \quad \partial_1\mathcal{D}, \tag{14}$$

where $\boldsymbol{n}$ stands for the outward unit normal on $\partial\mathcal{D}$, $u_n = \boldsymbol{u}\cdot\boldsymbol{n}$ is normal velocity, $\boldsymbol{\sigma}_t = \boldsymbol{\sigma} - (\boldsymbol{\sigma}\cdot\boldsymbol{n})\boldsymbol{n}$ stands for the tangential stress and $\mathbf{V}$ is the imposed velocity.

A slip-dependent frictional contact is assumed on the boundary $\partial_2\mathcal{D}$

$$u_n = 0, \qquad \begin{cases} \boldsymbol{u}_t = 0 \implies |\boldsymbol{\sigma}_t| \leq \mu|\sigma_n|, \\ \boldsymbol{u}_t \neq 0 \implies \boldsymbol{\sigma}_t = -\mu|\sigma_n|\dfrac{\boldsymbol{u}_t}{|\boldsymbol{u}_t|}, \end{cases} \tag{15}$$

where $\sigma_n = \boldsymbol{\sigma n}\cdot\boldsymbol{n}$ is the normal stress, $\boldsymbol{u}_t = \boldsymbol{u} - u_n\boldsymbol{n}$ is the tangential velocity and μ is the friction coefficient. According to (15), the the tangential (friction) stress is bounded by the normal stress multiplied by the friction coefficient μ. If such a limit is not attained sliding cannot occur; otherwise the friction stress is opposite to the slip rate. The friction coefficient will be considered variable during the slip. Experimental observations indicate that the friction coefficient depends on the slip rate $|\boldsymbol{u}_t|$ i.e. $\mu = \mu(|\boldsymbol{u}_t|)$. The simplest law of variation of μ on the slip rate is a discontinuous jump from a "static" value (for $|\boldsymbol{u}_t| = 0$) down to a "dynamic" or "kinetic" value (for $|\boldsymbol{u}_t| \neq 0$). In this work, we will consider a smooth and decreasing function $\mu = \mu(|\boldsymbol{u}_t|)$ of the slip rate.

The boundary condition for the conservation of mass equation is:

$$\rho = \rho_0 \quad \text{on} \quad \partial_\rho\mathcal{D} \tag{16}$$

i.e. a given density is prescribed on $\partial_\rho\mathcal{D} \subset \partial\mathcal{D}$.

Setting

$$V = \left\{\boldsymbol{v} \in H^1(\mathcal{D})^3; \boldsymbol{v} = \mathbf{V} \ \text{ on } \partial_0\mathcal{D},\ v_n = 0 \ \text{ on } \partial_2\mathcal{D}\right\}, \quad \mathcal{V} = \left\{\boldsymbol{v} \in V;\ \operatorname{div}\boldsymbol{v} \leq 0 \ \text{ in } \mathcal{D}\ \right\}$$

the kinematic admissible set, the variational formulation for the velocity field $\boldsymbol{u} \in \mathcal{V}$ is:

$$\begin{aligned} &\int_{\mathcal{D}} \rho(\boldsymbol{u}\cdot\nabla)\boldsymbol{u}\cdot(\boldsymbol{v}-\boldsymbol{u}) + \int_{\mathcal{D}} 2\eta(\rho)D'(\boldsymbol{u}) : (D'(\boldsymbol{v}) - D'(\boldsymbol{u})) + \\ &\int_{\mathcal{D}} \kappa(\rho)(|D'(\boldsymbol{v})| - |D'(\boldsymbol{u})|) + \int_{\mathcal{D}} [(\lambda(\rho) + \frac{2}{3}\eta(\rho))\operatorname{div}\boldsymbol{u} - p(\rho)]\operatorname{div}(\boldsymbol{v}-\boldsymbol{u}) \\ &\qquad + \int_{\partial_2\mathcal{D}} \mu(|\boldsymbol{u}_t|)|\sigma_n|(|\boldsymbol{v}_t| - |\boldsymbol{u}_t|) \geq \int_{\mathcal{D}} \rho\boldsymbol{f}\cdot(\boldsymbol{v}-\boldsymbol{u}). \end{aligned} \tag{17}$$

for all $\boldsymbol{v} \in \mathcal{V}$.

Thus, the problem of the flow of compressible visco-plastic Bingham-type fluid becomes:

Find the velocity field $\boldsymbol{u}$ and the mass density field ρ such that equations (13), and (17) hold.

4 Numerical approach

In this section, we present the numerical approach adopted for solving the problem of the stationary flow of a rigid-viscoplastic Bingham type material.

The algorithm consists of solving alternatively the variational inequality (17) for the velocity field and the continuity equation (13) for the density field. More precisely, we shall distinguish two problems : the "velocity problem" and the the "density problem". For the velocity problem we assume that ρ and the distributions of p, η, λ and κ are given, and we find $\boldsymbol{u} \in \mathcal{V}$, the solution of (17). The density problem consists in finding the density field ρ solution of (13) assuming that $\boldsymbol{u}$ is given.

As it follows from the next subsection the velocity problem will be solved by an iterative procedure. At each iteration k we get a velocity field $\boldsymbol{u}^k$ which will be used to solve the density problem

$$\operatorname{div}(\rho^k \boldsymbol{u}^k) = 0 \quad \text{in } \mathcal{D}, \qquad \rho^k = \rho_0 \quad \text{on} \quad \partial_\rho \mathcal{D} \tag{18}$$

and getting ρ^k to update the density field.

4.1 The velocity problem

Suppose that $\mathcal{D}$ is discretized by using a family of triangulations $(\mathcal{T}_h)_h$ made of finite elements of degree 2 where $h > 0$ is the discretization parameter representing the greatest diameter of a triangle in $\mathcal{T}_h$. The finite element space V_h, which is an internal appoximation of V reads:

$$V_h = \Big\{ \boldsymbol{v}_h;\ \boldsymbol{v}_h \in \big(C(\overline{\mathcal{D}})\big)^3,\ \boldsymbol{v}_h|_T \in \big(P_2(T)\big)^3\ \ \forall T \in \mathcal{T}_h,\ \boldsymbol{v}_h = \mathbf{V}\ \text{ on } \partial_0\mathcal{D},\ v_{hn} = 0\ \text{ on } \partial_2\mathcal{D} \Big\},$$

where $C(\overline{\mathcal{D}})$ stands for the space of continuous functions on $\overline{\mathcal{D}}$ and $P_i(T)$ represents the space of polynomial functions of degree i on T.

Let $\mathcal{V}_h = \mathcal{V} \bigcap V_h$. Then, the velocity problem is discretized by considering $\boldsymbol{u}_h \in \mathcal{V}_h$ which satisfies (17) for all $\boldsymbol{v} \in \mathcal{V}_h$. In order to simplify the notations we shall omit in all this subsection the indexes h.

For all $\boldsymbol{w} \in \mathcal{V}_h$ let $J_{\boldsymbol{w}} : V_h \to \mathbb{R}$ be given by

$$J_{\boldsymbol{w}}(\boldsymbol{v}) = \int_{\mathcal{D}} \eta |D'(\boldsymbol{v})|^2 + \int_{\mathcal{D}} \left(\frac{1}{2}\lambda + \frac{1}{3}\eta\right)(\operatorname{div} \boldsymbol{v})^2 + \int_{\mathcal{D}} \kappa |D'(\boldsymbol{v})| + \int_{\partial_2\mathcal{D}} \mu(|\boldsymbol{w}_t|)|\sigma_n(\boldsymbol{w})||\boldsymbol{v}_t|$$
$$+ \int_{\mathcal{D}} \rho(\boldsymbol{w}\cdot\nabla)\boldsymbol{w}\cdot\boldsymbol{v} - \int_{\mathcal{D}} p \operatorname{div} \boldsymbol{v} - \int_{\mathcal{D}} \rho \boldsymbol{f}\cdot\boldsymbol{v}. \tag{19}$$

Hence, the velocity problem can be written as

$$\boldsymbol{u} \in \mathcal{V}_h, \quad J_{\boldsymbol{u}}(\boldsymbol{u}) = \inf_{\boldsymbol{v}\in\mathcal{V}_h} J_{\boldsymbol{u}}(\boldsymbol{v}) \tag{20}$$

The following iterative algorithm is proposed : given $\boldsymbol{u}^{k-1} \in \mathcal{V}_h$ find $\boldsymbol{u}^k \in \mathcal{V}_h$, the solution of the following minimization problem

$$\boldsymbol{u}^k \in \mathcal{V}_h, \quad J_k(\boldsymbol{u}^k) = \inf_{\boldsymbol{v}\in\mathcal{V}_h} J_k(\boldsymbol{v}), \qquad J_k(\boldsymbol{v}) = J_{\boldsymbol{u}^{k-1}}(\boldsymbol{v}) \tag{21}$$

Since J_k is not Gâteaux differentiable, one can use (see for instance [17, 18, 5]) the function $\varphi_\epsilon(x) = \sqrt{(x^2+\epsilon^2)} - \epsilon$ to regularize the euclidian norm of the second order tensors. With

this technique, the material is not completely rigid anymore, and so it is difficult to capture accurately the shape of the rigid zone. In this paper, we use a decomposition-coordination formulation coupled with the augmented lagrangian method (see [14, 13]). This approach is accurate in detecting the visco-plastic regions and permit us to handle the locking condition.

Let

$$\Delta_h = \Big\{ \boldsymbol{\delta}_h;\ \boldsymbol{\delta}_h \in L^2(\overline{\mathcal{D}})^3,\ \boldsymbol{\delta}_h|_T \in P_1(T)^3\ \ \forall T \in \mathcal{T}_h,\ \Big\},$$

$$\Theta_h = \Big\{ \theta_h;\ \theta_h \in L^2(\overline{\mathcal{D}}),\ \theta_h|_T \in P_1(T)\ \ \forall T \in \mathcal{T}_h,\ \Big\}$$

and the Lagrangian L_k^ϵ:

$$\begin{aligned} L_k(\boldsymbol{v},\boldsymbol{\sigma},\theta,\boldsymbol{\delta}) = \int_{\mathcal{D}} \eta|\boldsymbol{\delta}|^2 + \int_{\mathcal{D}} \left(\frac{1}{2}\,\lambda + \frac{1}{3}\,\eta\right)\theta^2 + \int_{\mathcal{D}} \kappa|\boldsymbol{\delta}|\ - \int_{\mathcal{D}} p\ \theta\ + \\ \int_{\partial_2\mathcal{D}} \mu(|\boldsymbol{u}_t^{k-1}|)|\sigma_n(\boldsymbol{u}^{k-1})| \frac{\boldsymbol{u}_t^{k-1}\cdot\boldsymbol{v}_t}{\sqrt{|\boldsymbol{u}_t^{k-1}|^2+\epsilon^2}} + \int_{\mathcal{D}} \rho(\boldsymbol{u}_{k-1}\cdot\nabla)\boldsymbol{u}_{k-1}\cdot\boldsymbol{v} - \int_{\mathcal{D}} \rho\boldsymbol{f}\cdot\boldsymbol{v}\ + \\ \int_{\mathcal{D}} (D'(\boldsymbol{v})-\boldsymbol{\delta}) : \boldsymbol{\sigma}'\ +\ \int_{\mathcal{D}} (\theta - \operatorname{div}\boldsymbol{v})\cdot \operatorname{trace}\ \boldsymbol{\sigma} \end{aligned} \tag{22}$$

where $\boldsymbol{v} \in V_h$, $\boldsymbol{\delta} \in \Delta_h$ represents $D'(\boldsymbol{v})$, $\theta \in \Theta_h$ stands for $\operatorname{div}\boldsymbol{v}$ and the lagrangian multiplier $\boldsymbol{\sigma} \in \Delta_h$ is the stress inside the material. Let us introduce the augmented Lagrangian $\mathcal{L}_k$:

$$\mathcal{L}_k(\boldsymbol{v},\boldsymbol{\sigma},\theta,\boldsymbol{\delta}) = L_k(\boldsymbol{v},\boldsymbol{\sigma},\theta,\boldsymbol{\delta})\ +\ r_D \int_{\mathcal{D}} |D'(\boldsymbol{v})-\boldsymbol{\delta}|^2\ +\ r_H \int_{\mathcal{D}} |\ \theta - \operatorname{div}\boldsymbol{v}|^2, \tag{23}$$

where r_H and r_D are strictly positive constants. As it follows from [14, 13] $\mathcal{L}_k$ is quadratic with respect with $\boldsymbol{v}$ and its saddle points coincide with those of L_k. Thus, the minimization problem (21) becomes: find $u^k \in \mathcal{V}_h$, $\boldsymbol{\sigma}^k \in \Delta_h$, $\theta^k \in \Theta_h$ and $\boldsymbol{\delta}^k \in \Delta_h$ such that

$$\sup_{\theta,\boldsymbol{\sigma},\boldsymbol{\delta}} \mathcal{L}_k(\boldsymbol{u}^k,\boldsymbol{\sigma},\theta,\boldsymbol{\delta}) \le \mathcal{L}_k(\boldsymbol{u}^k,\boldsymbol{\sigma}^k,\theta^k,\boldsymbol{\delta}^k) \le \inf_{\boldsymbol{v}\in\mathcal{V}_h} \mathcal{L}_k(\boldsymbol{v},\boldsymbol{\sigma}^k,\theta^k,\boldsymbol{\delta}^k). \tag{24}$$

In order to solve the above saddle point problem we shall use an Uzawa-type algorithm (see [14]). For this let us put $\boldsymbol{\sigma}_0^{k-1} = \boldsymbol{\sigma}^{k-1}, \theta_0^{k-1} = \theta^{k-1}$ and $\boldsymbol{\delta}_0^{k-1} = \boldsymbol{\delta}^{k-1}$ and let us introduce two functions f_H and f_D useful in the description of the algorithm:

$$f_D(\boldsymbol{\sigma},a) \ = \ \frac{1}{2\eta(\rho)+a}\left[1-\frac{\kappa(\rho)}{|\boldsymbol{\sigma}'|}\right]_+ \boldsymbol{\sigma}' \tag{25}$$

$$f_H(\boldsymbol{\sigma},a) \ = \ \begin{cases} \left[\dfrac{3p(\rho)+\operatorname{tr}\boldsymbol{\sigma}}{3\lambda(\rho)+2\eta(\rho)+a}\right]_- & \text{if } \rho \le \rho^\star \\ 0 & \text{if } \rho > \rho^\star \end{cases} \tag{26}$$

where $[x]_+ = (x+|x|)/2$ and $[x]_- = (x-|x|)/2$ represent respectively the positive and the negative part. Let us remark that, by taking $a = 0$, (25) and (26) give us the complete model of our material:

$$D = f_D(\boldsymbol{\sigma},0) + \frac{f_H(\boldsymbol{\sigma},0)}{3} I_d = f(\boldsymbol{\sigma})$$

At the iteration i, we know $\boldsymbol{\sigma}_{i-1}^{k-1}, \boldsymbol{\delta}_{i-1}^{k-1}, \theta_{i-1}^{k-1}$ and we compute $\boldsymbol{u}_i^{k-1}, \boldsymbol{\sigma}_i^{k-1}, \boldsymbol{\delta}_i^{k-1}, \theta_i^{k-1}$ as follows

$$\boldsymbol{u}_i^{k-1} \in V_h, \qquad \mathcal{L}_k(\boldsymbol{u}_i^{k-1},\boldsymbol{\sigma}_{i-1}^{k-1},\theta_{i-1}^{k-1},\boldsymbol{\delta}_{i-1}^{k-1}) = \inf_{\boldsymbol{v}\in V_h} \mathcal{L}_k(\boldsymbol{v},\boldsymbol{\sigma}_{i-1}^{k-1},\theta_{i-1}^{k-1},\boldsymbol{\delta}_{i-1}^{k-1}).$$

$$\boldsymbol{\delta}_i^{k-1} = f_D\big(\boldsymbol{\sigma}_{i-1}^{k-1} + 2r_D D(\boldsymbol{u}_i^{k-1}), 2r_D\big), \quad \theta_i^{k-1} = f_H\big(\boldsymbol{\sigma}_{i-1}^{k-1} + 2r_H D(\boldsymbol{u}_i^{k-1})), 2r_H\big)$$

$$(\boldsymbol{\sigma}_i^{k-1})' = (\boldsymbol{\sigma}_{i-1}^{k-1})' + 2r_D\big(D'(\boldsymbol{u}_i^{k-1}) - \boldsymbol{\delta}_i^{k-1}\big), \quad \operatorname{trace}\boldsymbol{\sigma}_i^{k-1} = \operatorname{trace}\boldsymbol{\sigma}_{i-1}^{k-1} + 2r_H\big(div\boldsymbol{u}_i^{k-1} - \theta_i^{k-1}\big).$$

For large enough $i = i^{max}$ we put $u^k = u_{i^{max}}^{k-1}, \boldsymbol{\sigma}^k = \boldsymbol{\sigma}_{i^{max}}^{k-1}, \theta^k = \theta_{i^{max}}^{k-1}$ and $\boldsymbol{\delta}^k = \boldsymbol{\delta}_{i^{max}}^{k-1}$. The interest of this algorithm is that it transforms the non-differentiable problem into a sequence of completely standard computations.

We shall use in the numerical results presented in the next sections a single pass (i.e. $i^{max} = 1$) Uzawa-type algorithm to deduce the following numerical approach for the velocity problem.

A). The algorithm starts with arbitraries $\boldsymbol{\sigma}^0$, θ^0 and $\boldsymbol{\delta}^0$.

B). At the iteration k, we have $\boldsymbol{\sigma}^{k-1}$, $\boldsymbol{\delta}^{k-1}$ and θ^{k-1}. From the previous density problem we know also the density ρ^{k-1}, and therefore the distributions of p, η, λ and κ. Then we have to compute the following three steps:

1 − **First Step:**

$$\text{find } \boldsymbol{u}^k \in V_h \quad \text{such that} \quad \mathcal{L}_k(\boldsymbol{u}^k, \boldsymbol{\sigma}^{k-1}, \theta^{k-1}, \boldsymbol{\delta}^{k-1}) = \inf_{\boldsymbol{v}\in V_h} \mathcal{L}_k(\boldsymbol{v}, \boldsymbol{\sigma}^{k-1}, \theta^{k-1}, \boldsymbol{\delta}^{k-1}). \tag{27}$$

This problem is equivalent to find u^k such that:

$$-\,\mathbf{div}\,\big(2\, r_D D'(u^k) + \frac{2}{3} r_H \operatorname{div}(u^k) I_3\big) \;=\; \mathbf{div}\,\big(\boldsymbol{\sigma}^{k-1} \;-\; 2r_D\boldsymbol{\delta}^{k-1} \;-\; \frac{2}{3} r_H \theta^{k-1} I_3\big) +$$

$$\rho^{k-1}\big((\boldsymbol{u}^{k-1}\cdot\nabla), \boldsymbol{u}^{k-1} - \boldsymbol{f}\big),$$

with appropriate boundary conditions.

2 − **Second Step:** Compute explicitly θ^k and $\boldsymbol{\delta}^k$ using the constitutive equations (25) and (26):

$$\begin{cases} \boldsymbol{\delta}^k = f_D\big(\boldsymbol{\sigma}^{k-1} + 2r_D D(\boldsymbol{u}^k), 2r_D\big), \\ \theta^k = f_H\big(\boldsymbol{\sigma}^{k-1} + 2r_H D(\boldsymbol{u}^k), 2r_H\big). \end{cases}$$

3 − **Third Step:** Compute $\boldsymbol{\sigma}^k$ through the following formulas:

$$\begin{cases} (\boldsymbol{\sigma}^k)' = (\boldsymbol{\sigma}^{k-1})' + 2r_D\big(D'(\boldsymbol{v}^k) - \boldsymbol{\delta}^k\big), \\ \operatorname{trace}\boldsymbol{\sigma}^k = \operatorname{trace}\boldsymbol{\sigma}^{k-1} + 2r_H\big(\operatorname{div}\boldsymbol{v}^k - \theta^k\big). \end{cases}$$

C). The algorithm stops when $\dfrac{||\boldsymbol{u}^k - \boldsymbol{u}^{k-1}||_{L^2(\mathcal{D})}}{||\boldsymbol{u}^k||_{L^2(\mathcal{D})}}$ is small enough.

4.2 The density problem

A finite volume method (see for instance [12]) will be used to discretize equation (18). Let denote by $\mathcal{K}_h$ the finite volume mesh, which is given by a family of disjoint polygonal connected subsets of $\mathbb{R}^3$ such that $\overline{\mathcal{D}}$ is the union of the closure of the elements of $\mathcal{K}_h$; h is the greatest

diameter of a control volume in $\mathcal{K}_h$. The finite volume mesh $\mathcal{K}_h$ is obtained from a finite element triangulation $\mathcal{T}_h$. In two space dimensions, the middle of each side of a triangle T is connected to the center of mass to obtain three pieces. A control volume $K \in \mathcal{K}_h$, which corresponds to the node A, is obtained from the union of all pieces which have the node A.

The finite volume discrete space is the space of piecewise constant functions, i.e. we are looking for the solution ρ_h^k of (18) as $\{\rho_{hK}^k,\ K \in \mathcal{K}_h\}$. In order to simplify the notations we shall omit in all this subsection the indexes h and k and ρ_h^k and $\boldsymbol{u}_h^k$ will be denoted simply by ρ and $\boldsymbol{u}$.

Let us consider two control volumes $K, P \in \mathcal{K}_h$ with a common interface $I_{KL} = \overline{K} \bigcap \overline{P}$. Let $\boldsymbol{n}$ be the unit normal vector to I_{KP} oriented from K to P. The we define the flux $F(K,P)$ at the interface I_{KP} as

$$F(K,P) = \int_{I_{KP}} [\boldsymbol{u} \cdot \boldsymbol{n}]_+.$$

Note that at least one of the two fluxes $F(K,P)$ and $F(P,K)$ is vanishing. If we denote by $\mathcal{N}(K)$ the set of all neighbors of the control volume K then the finite volume numerical scheme for (18) reads as a linear algebraic system for the unknowns $(\rho_K)_{K \in \mathcal{K}_h}$

$$\sum_{P \in \mathcal{N}(K)} F(K,P)\rho_K - F(P,K)\rho_P = 0, \qquad \text{for all} \quad K \in \mathcal{K}_h. \tag{28}$$

If a volume control L corresponds to a node which is on the boundary $\partial_\rho \mathcal{D}$ then we put $\rho_P = \rho_0$ and we eliminate the corresponding equation.

5 Penetration in concrete

5.1 Material parameters model

To illustrate the predictive capabilities of the model, its application to concrete is presented. The data available consists of laboratory quasi-static unconfined and confined compression tests for confining pressures in the range 50-450 MPa under a strain rate of 10-6/s and both confined and unconfined Split-Hopkinson bar data at strain rates of 60/s to 160/s. The ambient density of the material is:$\rho_0 = 2000\text{kgm}^{-3}$ and the unconfined strength is of 60.00 MPa(data after Schmdit[29]. The locking density is of $\rho^* = 2,600$ kgm^{-3} and locking pressure $p^* = 0.5$ GPa.

The pressure - density relationship for this material can be approximated by

$$\begin{cases} p(\rho) & = p^* \dfrac{\rho^*}{\rho^* - \rho_0}(1 - \dfrac{\rho_0}{\rho}), & \text{if } \rho_0 \le \rho < \rho* \\ p(\rho) & \ge p^*, & \text{if } \rho \ge \rho^* \end{cases} \tag{29}$$

The following law of variation of the yield limit with the current density describes well the data:

$$\kappa(\rho) = \kappa_0 + \beta(1 - \frac{\rho_0}{\rho})$$

where $\beta = (\kappa^* - \kappa_0)\rho_0/(\rho^* - \rho_0)$ and κ_0, κ^* are the yield stress corresponding to the density of the undeformed ($\rho = \rho_0$) and locked medium ($\rho = \rho^*$). In the numerical simulations, we have taken $\kappa_0 = 100MPa$, and $\kappa^* = 800MPa$.

For the viscosity coefficients $\eta(\rho)$ and $\lambda(\rho)$ a similar variation law as for the yield limit is used

$$\eta(\rho) = \eta_0 + \gamma(1 - \frac{\rho_0}{\rho})^2, \qquad \lambda(\rho) = \lambda_0 + \boldsymbol{\delta}(1 - \frac{\rho_0}{\rho})^2,$$

where $\gamma = (\eta^* - \eta_0)(\rho_0/(\rho^* - \rho_0))^2$ and $\boldsymbol{\delta} = (\lambda^* - \lambda_0)(\rho_0/(\rho^* - \rho_0))^2$. The set of values chosen in the numerical simulations are: $\eta_0 = 20.$ kPa·s,$\eta^* = 5.$ kPa·s, $\lambda_0 = 10$ kPa·s and $\lambda^* = 1.0$ MPa·s.

5.2 Boundary conditions

On the boundary $\partial_0\mathcal{D}$, which consists of the polygonal line $OFEC$, the velocity is $V\mathbf{e_z}$, where $\mathbf{V}$ is the impact velocity. Simulations were performed for an impact velocity of 500 ms $^{-1}$. Since the control volume $\mathcal{D}$ does not touch the tunnel we have $\partial_1\mathcal{D} = \emptyset$. Preliminary simulations, in which a part of the tunnel was modelled have shown that the material in $\mathcal{D}$ which is behind the projectile is rigid and thus does not influence the computations.

The frictional contact boundary is the boundary of the projectile, i.e. ABC on the figure 1. We have chosen Lim-Ashby-Klepaczko model (see [20]) to describe the influence of the velocity on the friction coefficient between the concrete target and the metallic penetrator

$$\mu(v) = a[1 - b\log(1 + \frac{v}{v_0})]$$

where $a = 0.5$, $b = 0.263$ and $v_0 = 1.0$ ms^{-1}. The boundary condition $u_n = 0$ prescribed on the projectile is accurate everywhere apart from two small zones. The first one is located on the nose of the projectile in the neighborhood of A. In this zone, rupture in the target material and creation of a free boundary, which begins somewhere on OA and ends somewhere on AB, but still very close to A is to be expected. In the second zone, which is located on the body of the projectile behind and near B, the target material is no longer in contact with the projectile. This corresponds to a second free boundary zone which starts and ends somewhere on the body BC. The formulation and solution of these two free boundary problems is beyond the scope of this study. However, the influence of these two zones on the resistance to penetration seems to be very small.

5.3 Mesh adaptation

In order to capture sharply the shape of the visco-plactic zone, we have used the anisotropic mesh generator $BAMG$ (see [15, 16]). This generator requires a governing field for re-meshing and refines the zones with high second derivative. The field E we used is the square root of the dissipative energy associated to a velocity field $\boldsymbol{u}$ computed through $\boldsymbol{\delta}$ and θ defined in (22).

$$E = \sqrt{\boldsymbol{\sigma}(\boldsymbol{u}) : D(\boldsymbol{u})} = \sqrt{\eta(\rho)|\boldsymbol{\delta}|^2 + \kappa(\rho)|\boldsymbol{\delta}| - p(\rho)\theta + \frac{2\eta(\rho) + 3\lambda(\rho)}{3}\,\theta} \tag{30}$$

Note that E is continuous, but its first derivative is discontinuous across the zones of contact between the rigid and visco-plastic regions; that means that the second derivative is very large on this surface that the mesh generator will emphasize this boundary. Other regions have to be refined, those ones with high rates of deformation. As we can expect, the zone around the nose of the projectile will be also privileged.

In figure 2 we have plotted the initial finite element mesh of the domain $OABCEF$, and the distribution of the deformation rate $|D(\boldsymbol{u})|$. Note that the boundary between the rigid zone

and the visco-plastic one is not well captured. This mesh has 2304 nodes and 4356 triangular elements. The finite element mesh obtained after remeshing is plotted in Figure 3. Using 6992 nodes and 13,719 triangular elements this mesh is able to give a satisfactory description of the rigid zone.

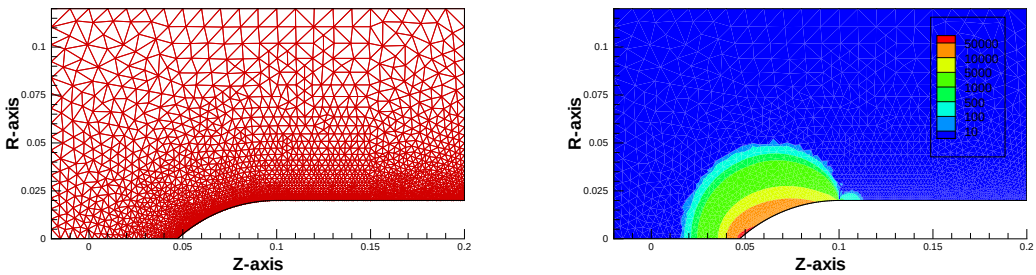

Figure 2: The initial finite element mesh (left), and the distribution of the deformation rate $|D(\boldsymbol{u})|$ (right). Note that the boundary between the rigid zone and the visco-plastic one is not well captured.

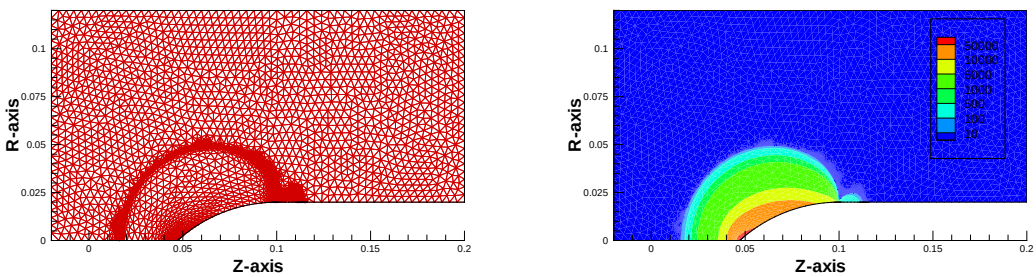

Figure 3: The finite element mesh obtained after remeshing (left), and the distribution of the deformation rate $|D(\boldsymbol{u})|$ (right). Note that the boundary between the rigid zone and the visco-plastic one is sharply captured.

6 Results and discussion

Figure 4 shows the distribution of density in the target. Note the existence of three distinct zones: (1) a fully compacted zone around the penetrator, where the density is everywhere equal to the locking density ρ_* , (2) a compacted where the density varies between ρ_0, the density of the intact material, and ρ_*; (3) a zone that remains unaffected by the impact event where the density is everywhere equal to ρ_0. The streamlines are shown in figure streamlines. It is worth noticing that all the particles ahead of the projectile which are at a distance from the centerline less than R will enter the fully compacted zone (1).

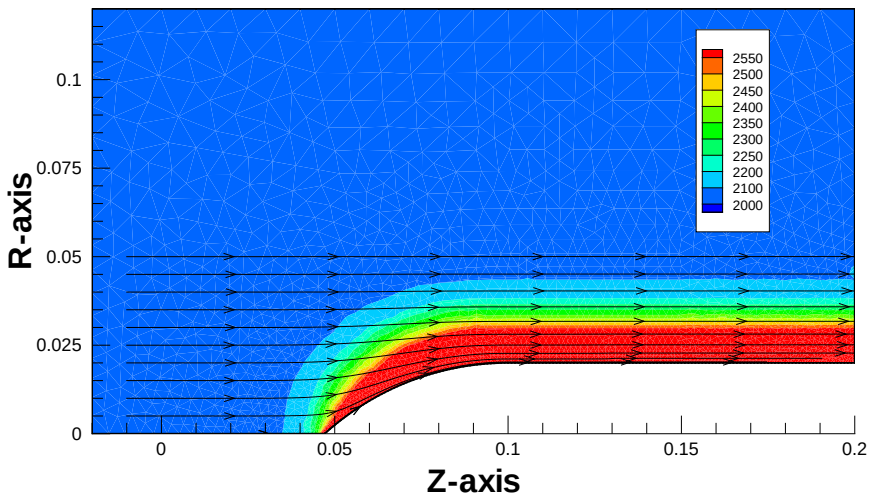

Figure 4: The distribution of density in the target and the streamlines computed in Kg m^{-3}.

In figure 5 it is shown the distribution of the second invariant of the rate of deformation deviator $|D'(\boldsymbol{u})|$. It is seen that a zone of intense plastic deformation develops around the penetrator and it extends outward to approximatively 3 projectile radii from the centerline. The maximum rate of deformation is achieved on the nose tip. Outside this zone, $|D'(\boldsymbol{u})|$ vanishes, hence according to the model no plastic deformation can occur.

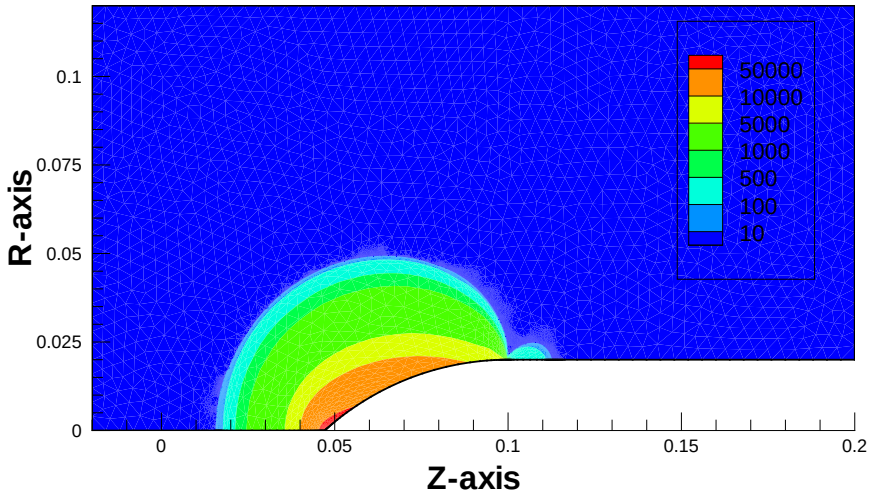

Figure 5: The distribution of the second invariant of the rate of deformation deviator $|D'(\boldsymbol{u})|$ computed in s^{-1}.

The distribution of the rate of volumetric deformation $\operatorname{div} \boldsymbol{u}$ is displayed in Figure 6. We note that around the penetrator, a fully compacted state is achieved, the maximum compaction being in the nose zone. Because the prescribed boundary conditions do not reflect that the target material is not in contact with the projectile on a limited zone of the body of the projectile, $\operatorname{div} \boldsymbol{u}$ is slightly positive in a small region behind the projectile. This zone corresponds to positive normal stresses. This can be seen in Figure 7 where it is shown the distribution of the normal stress σ_n along the projectile. High compressive values on the tip of the nose and very small values on the shank are obtained. The tangential velocity $\boldsymbol{u}_t$ on the projectile, plotted in Figure 7, is very small on the tip and gradually increases until it reaches the value of the impact velocity on the shank.

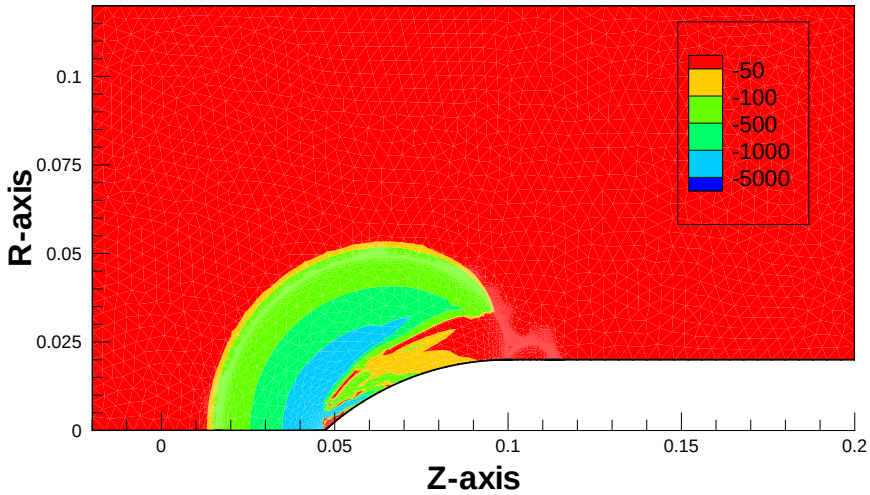

Figure 6: The distribution of the rate of volumetric deformation div $\boldsymbol{u}$ computed in s^{-1}.

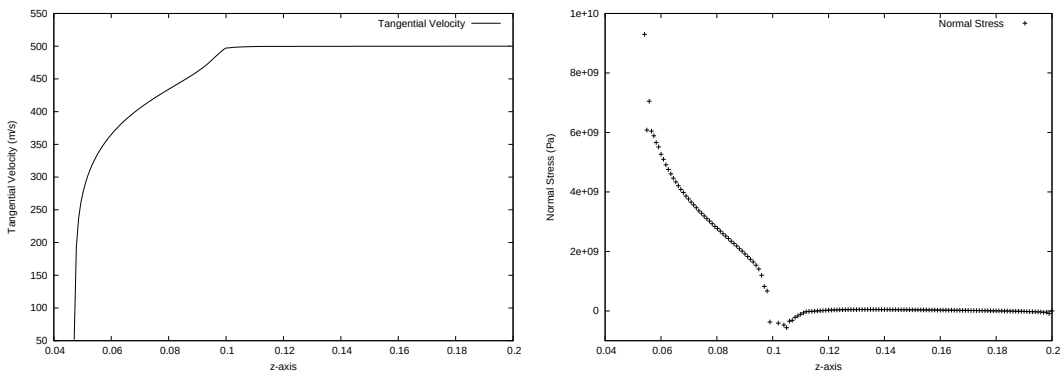

Figure 7: Left: the distribution of tangential velocity $\boldsymbol{u}_t$ along the projectile computed in ms^{-1}. Right : The distribution of the normal stress σ_n along the projectile computed in Pa.

Let us analyze now the stress distribution in the target and determine the zones where tensile failure may occur. It is assumed that concrete tensile failure can be modelled with the

classic maximum tensile strength criterion (see [25]), i.e. the material fails if the maximum of the principal stresses reaches a critical limit denoted f. The tensile strength depends on the level of compaction of the material. A power law variation of this tensile strength of the material with the current density is assumed

$$f(\rho) = f_0 + a(1 - \frac{\rho_0}{\rho})^2$$

where $a = (f^* - f_0)(\rho_0/(\rho^* - \rho_0))^2$ and f_0, f^* are the tensile strength corresponding to the density of the non deformed ($\rho = \rho_0$) and locked medium ($\rho = \rho^*$). For the numerical tests we have used $f_0 = 33.3MPa$, and $f^* = 233.3MPa$. The plot of the distribution of $\sigma_{\theta\theta}/f$ is plotted in figure 8. We remark that in a wide region ahead of the projectile the tensile failure can occur along Ozr planes orthogonal to $\mathbf{e}_{\theta\theta}$ (see figure 1). Following the stream lines a part of this region will be fully compacted, hence in the lagrangian configuration fracture will not be observed near the projectile.

From the analysis of the spatial distribution of damage in the target one can gain fundamental understanding of the stability of the penetrator trajectory. We have found that damage occurs ahead the projectile and along planes which can be not symmetric with respect to the penetrator centerline. This damage induced anisotropy can explain trajectory deviations.

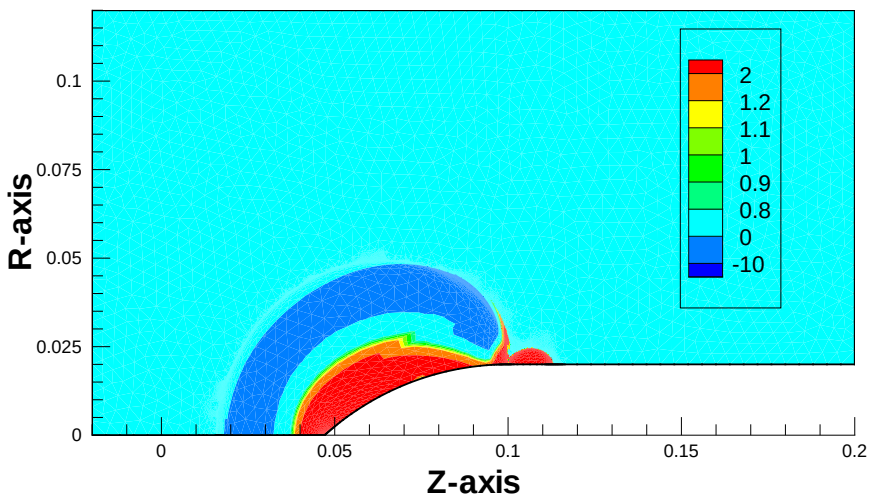

Figure 8: The distribution of $\sigma_{\theta\theta}/f$ in the target.

7 Conclusions

A model for describing steady-state penetration of a rigid penetrator into a geologic or geologically derived material was proposed.

Since for low-to-intermediate impact velocities, the impacted medium displays both solid-like and fluid-like behavior a rigid visco-plastic fluid type constitutive was developed. To capture the observed dependence of yielding and strain-rate sensitivity on compaction, an explicit dependence of the yield limit and viscosity coefficients on density was considered. To reflect the observed characteristics of the pressure-density relationships in geologic materials when subjected to high-pressure (of the order of GPa) the hypothesis of rigid unloading and locking medium was adopted (i.e. the density cannot exceed a critical limit). Variational formulations and algorithms for solving the minimization problems for the velocity field using the finite element method were developed while finite-volume techniques were adopted for solving the hyperbolic mass conservation equation. To solve the velocity problem a decomposition-coordination formulation coupled with the augmented lagrangian method is used. The model was applied to penetration into concrete. The deformation behavior was described using the viscoplastic compressible fluid model developed while fracture was modeled using the classic maximum tensile stress criterion. The model predicts that around the penetrator, a fully compacted state is achieved, the maximum compaction being in the nose zone. Fracture occurs ahead of the penetrator and along planes which can be not symmetric with respect to the penetrator centerline. This induced anisotropy can explain trajectory deviations.

References

[1] V. Adamik and P.Matejovic (1989) "A contribution to computational modeling of reinforced concrete structures subjected to impact loading.", *Nuclear Engrg. Des.*, 113, pp. 111-120.

[2] R. C. Batra (1987) "Steady-state penetration of viscoplastic targets", *Int.J.Engng.Sci.* 25, pp. 1131-1141.

[3] E.C. Bingham, *Fluidity and plasticity*, Mc Graw-Hill, New-York, (1922).

[4] O. Cazacu and N. Cristescu(2000) "Constitutive model and analysis of creep flow of natural slopes", *Italian Geotechnical Journal* 34 (3), pp. 44-54.

[5] O.Cazacu, I.R.Ionescu and T.Perrot (2004) Penetration of a rigid body into into a viscoplastic compressible fluid, to appear in *ECCOMAS 2004 Proceedings*

[6] F. Camborde, C. Mariotti, and F. V. Donze(2000), Numerical study of rock and concrete behavior by discrete element modelling, *Computer and Geotechnics* 27, pp. 225-247.

[7] O. Cazacu and N. Cristescu (2004), "Steady flow of a non-homogeneous Bingham material over a wedge", submitted Int. J. Numer. and Analytical Methods in Geomech.

[8] N. Cristescu, *Dynamic Plasticity*, Noth Holland, 1967

[9] N. Cristescu, On the optimal die angle in fast wire drawing, *Journal of Mechanics and Working Technology*, 3 (1980), 275–287.

[10] F. V. Donze, S. A. Magnier, L. Daudeville, C. Mariotti, and L. Davenne(1999) "Study of the behavior of concrete behavior at high strain rate compression by a discrete element method" *ASCE Journal of Engineering Mechanics* 125 (10), pp. 1154-1163.

[11] S.A. Elaskar and L.A. Godoy, Constitutive relations for compressible granular materials using non-nowtonian fluid mechanics, *Int. J. Mech. Sci.* Vol. 40, no 10, 1001–1081, 1998

[12] R. Eymard, T. Gallouet, R. Herbin, "The finite volume method", *Handbook for Numerical Analysis*, Ph. Ciarlet J.L. Lions eds, North Holland, 2000, 715-1022.

[13] M. Fortin and R. Glowinsky "Methodes de Lagrangien augmentés, application á la résolution de problèmes aux limites", Dunod, 1982

[14] R. Glowinsky and P. Le Tallec "Augmented Lagrangian and Operator Splitting method in Non-Linear Mechanics", SIAM Studies in Applied Mathematics, 1989

[15] F.Hecht "Bidimesional anisotropic mesh generator", INRIA report, 1997.

[16] F.Hecht "BAMG: Bidimesional anisotropic mesh generator", INRIA report, 1998.

[17] I. R. Ionescu and M. Sofonea, *Functional and numerical methods in viscoplasticity.* Oxford Science Publications. The Clarendon Press, Oxford University Press, New York, (1993).

[18] I. Ionescu and B. Vernescu, A numerical method for a viscoplastic problem. An application to the wire drawing, *Int. J. Engng. Sci.*, 26 (1988), 627–633.

[19] S. J. Jones, D.M.Jerome, L. Wilson, and F.R. Christopher(1998) " An engineering analysis of normal rigid body penetration into concrete" PVP-Vol 361,Structures Under Extreme Loading Conditions, ASME 1998, pp.63–67.

[20] J.R. Klepaczko, Surface Layer Thermodynamics of Steel Penetrators at high and very high velocities, Air Force research Laboratory, Munitions Directorate, Final report AFRL-MN-EG-TR-2002-7076,Eglin AFB

[21] L.E. Malvern and D.A. Jenkins Dynamic testing of laterally confined concrete. Technical Report ESL-TR-89-47, Air Force Engineering and Services Center. (1990)

[22] J.G. Oldroyd, A rational formulation of the equations of plastic flow for a Bingham solid, *Proc. Camb. Philos. Soc.*, 43 (1947) 100–105.

[23] G. N. Pande, G. Beer, and J. R. Williams *Numerical Methods in Rock Mechanics* John Wiley & Sons, West Sussex, England,1990.

[24] O. Pironneau, *Finite element methods for fluids*, John Wiley & Sons Ltd., Chichester, 1989

[25] W. Rankine, *Applied Mechanics*, Charles Griffin and Company, London, 1972.

[26] C.A. Ross, D. M. Jerome, J.W. Tedesco, and M.L. Hughes (1996) "Moisture and strain rate effects in concrete". *ACI Materials Journal*, 93(3), pp. 293-300.

[27] L.E. Schwer, R. Rosinsky, and J. Day, (1988) "An axisymmetric Lagrangian technique for predicting earth penetration including penetrator response" *Int. J. Numer. and Analytical Methods in Geomech.*, 12, pp. 235-262.

[28] M.J. Schmidt, O. Cazacu, C.A. Ross, and N.D. Cristescu (2001) "Dynamic behavior of mortar:experimental data and modeling", *Proceedings of the 10th International Conference on Computer Methods and Advances in Geomechanics*, Tucson, Arizona.

[29] M.J. Schmidt (2003) High-Pressure and high-strain rate behavior of cementitious materials: experiments and elastic/viscoplastic modeling, Ph.D. Thesis, Univ. of Florida.

[30] R. Temam, *Navier-Stokes Equations. Theory and Numerical Analysis*, North-Holland, Amsterdam (1979).

[31] R. E. Tipton (1991) "Porous EOS in CALE used to model concrete" Lawrence Livermore National Laboratory, Livermore, CA.

[32] J.A. Zukas(1982) "Penetration and perforation of solids" in Impact Dynamics, John Wiley & Sons Inc, pp.155-214.